Applied Energy 328 (2022) 120195

Contents lists available at ScienceDirect

Applied Energy

journal homepage: www.elsevier.com/locate/apenergy

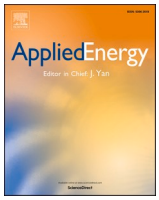

Multiple time-scale energy management strategy for a hydrogen-based multi-energy microgrid

Xiaolun Fang [a], Wei Dong [b], Yubin Wang [a], Qiang Yang [a,*]

[a] College of Electrical Engineering, Zhejiang University, Hangzhou 310027, China
[b] College of Automation, Hangzhou Dianzi University, Hangzhou 310018, China

HIGHLIGHTS

- A hydrogen-based MEMG in the electricity market is exploited.
- A multiple time-scale energy management solution for MEMG is developed.
- Electricity and hydrogen trading among subsystems are considered.
- Daily operational cost of the hydrogen-based MEMG is minimized.

ARTICLE INFO

Keywords:
Renewable energy
Fuel cell-based combined heat and power
Multiple time-scale energy management
Hydrogen-based multi-energy microgrid

ABSTRACT

With the technological advances in energy conversion and utilization of multiple forms of energy sources, hydrogen energy has attracted increasing attention. The hydrogen energy can be used to directly supply the hydrogen demand and generate both electricity and heat through fuel cell-based combined heat and power (FC-CHP) unit. This paper proposed a multiple time-scale energy management solution for a hydrogen-based multi-energy microgrid (MEMG) to supply electricity, hydrogen and heating loads aiming to minimize the MEMG operational cost with consideration of renewable energy generation and demand uncertainties. The proposed solution consists of day-ahead energy scheduling and model predictive control (MPC) based real-time energy dispatch in the presence of the electricity market. In the hydrogen-based MEMG, the electricity and hydrogen can be dispatched and utilized across multiple interconnected subsystems to improve the overall system energy utilization efficiency. The proposed solution is extensively assessed through simulation experiments compared with a benchmark solution. The numerical results confirm that the proposed solution outperforms the benchmark solution with the mean daily actual operational costs reduced by 37.08%.

1. Introduction

Hydrogen-based energy is considered a promising energy provision technology to reduce pollution emissions and energy crises [1]. Hydrogen production on-site using renewable energy (e.g. photovoltaic (PV) system) can realize low-carbon emissions [2]. Besides, in transportation systems, the use of plug-in electric vehicles (PEVs) and hydrogen fuel vehicles (HFVs) as an alternative to fossil fuel vehicles to mitigate the environmental pollution problem has attracted much attention [3]. However, the transition from fossil fuel vehicles to PEVs and HFVs depends on the widespread deployment of electric charging stations and hydrogen refueling stations. Thus, a hydrogen-based multi-energy microgrid (MEMG) with renewable energy is considered in this work, containing several interconnected subsystems, e.g., the electricity-hydrogen integrated charging stations (EHI-CSs) and park system. In the MEMG, EHI-CSs can supply both PEVs and HFVs demands and the park system can meet the electricity and heat demands. However, renewable generation exhibits intermittent and random characteristics and hence may not be able to fully meet the electricity demand

Abbreviations: PEV, Plug-in electric vehicle; HFV, Hydrogen fuel vehicle; MEMG, Multi-energy microgrid; EHI-CS, Electricity-hydrogen integrated charging station; P2H, Power-to-hydrogen; H2P, Hydrogen-to-power; MPC, Model predictive control; FC-CHP, Fuel cell-based combined heat and power; EL, Electrolyzer; EB, Electricity boiler; HSS, Heat storage system; PCC, Point of common coupling; LC, Local controller; DM, Day-ahead market; RTM, Real-time market; STS, Slow timescale; FTS, Fast timescale.

* Corresponding author.
E-mail address: qyang@zju.edu.cn (Q. Yang).

https://doi.org/10.1016/j.apenergy.2022.120195
Received 19 May 2022; Received in revised form 11 October 2022; Accepted 16 October 2022
Available online 27 October 2022

Nomenclature

Indices

t_s/t_f	Time slot index of STS/ FTS
m	Index of subsystems

Parameters and Constants

$\Delta t_s/\Delta t_f$	Time interval of STS/ FTS
t_s^{st}/t_f^{st}	Starting time interval in STS/ FTS of the current MPC round
T_s/T_f	Time slot numbers of STS/ FTS
P_m^{Solar}	Solar system power generation (MW)
H_m^{HFV}	HFVs demand (kg)
P_m^{PEV}	PEV fast charging demand (MW)
P^{Load}	Electrical demand of the park energy system (MW)
G^{Load}	Heat demand of the park energy system (MW)
$Y^{buy,e}/Y^{sell,e}$	Price of buying/ selling electricity of Day-ahead clearing price ($/MWh)
$Y_{sub}^{buy,H}/Y_{sub}^{sell,H}$	Price of buying/ selling hydrogen ($/kg)
$Y^{im,below}$	Negative imbalance price ($/MWh)
$Y^{im,excess}$	Positive imbalance price ($/MWh)
b^{P2H}/c^{P2H}	Cost function coefficient of the P2H mode ($/MWh)/ ($/h)
b^{CHP}	Cost function coefficients of the fuel cell FC-CHP unit ($/MWh)
f_L	Capacity of power line (MW)
E^{P2H}	P2H conversion factor (kg /kWh)
E^{H2P}	H2P conversion factor (kWh/ kg)
η^{EL}	Efficiency of the P2H unit(%)
$P_{max}^{P2H}/P_{min}^{P2H}$	Maximum/Minimum input electric power of the EL (MW)
HS_{max}/HS_{min}	The maximum/minimum value of hydrogen storage of the hydrogen tanks (kg)
$HS_{m,ini}$	Initial hydrogen storage value (kg)
H_{max}^{HESS}	Maximum charging and discharging hydrogen limit of hydrogen tanks (kg)
H_{max}^{trans}	The maximum hydrogen transportation (kg)
r^{H2P}	Hydrogen to electricity ratio of FC-CHP
d	Heat-to-electric ratio of FC-CHP
η^{EB}	Efficiency of EB (%)
G_{max}^{EB}	Maximum heat power generated by EB (MW)
GS_{max}/GS_{min}	The maximum/minimum value of heat storage of the heat storage tank (MW)
G_{max}^{HSS}	Maximum charging and discharging heat power limit of HSS (MW)
GS_{ini}	Initial heat power storage value (MW)

Variables

z	Time slot number of FTS in each time interval of STS
P_{grid}	Electrical power exchanged with the utility grid for the day-ahead schedule (MW)
P_{grid}^{act}	Actual electrical power exchanged with the utility grid (MW)
P_{grid}^{im}	Imbalance power of the deviation between the day-ahead schedule and real-time dispatch (MW)
$P_{used,m}^{Solar}$	PVs power generation utilized in actual (kW)
H_m^{EL}	Outflow hydrogen from P2H unit (kg)
P_m^{P2H}	Input power of P2H unit (MW).
I_m^{P2H}	Binary status indicator of P2H unit
HS_m	Stored hydrogen in the hydrogen tank (kg)
H^{CHP}	Hydrogen input of FC-CHP (kg)
P^{CHP}	Electricity generated from FC-CHP model (MW)
G^{CHP}	Heat power generated from FC-CHP model (MW)
P^{EB}	electrical power used by EB (MW)
G^{EB}	Heat power generated from EB (MW)
GS	Stored heat power in the heat storage tank (MW)
G^{ch}/G^{dis}	Charging and discharging heat power of HSS (MW)
$P_{grid}^{buy}/P_{grid}^{sell}$	Electrical power purchased/ sold from the utility grid (MW)
$P_{all,m}^{buy}/P_{all,m}^{sell}$	Total electrical power purchased/sold for the mth subsystem (MW)
$P_{sub,m}^{buy}/P_{sub,m}^{sell}$	Electrical power purchased/sold from the mth subsystem to other subsystems (MW)
$I_{grid}^{buy}/I_{grid}^{sell}$	Binary status indicator of electrical power purchased/ sold from the utility grid
$I_m^{H,buy}/I_m^{H,sell}$	Binary status indicator of hydrogen purchased/ sold from the mth subsystem
$H_{sub,m}^{buy}/H_{sub,m}^{sell}$	Hydrogen purchased/sold from the mth subsystem to other subsystems (kg)
$H_{sub,m_1m_2}^{trans}$	Hydrogen transfer from m_1th subsystem to m_2th subsystem (kg)

in MEMG. In addition, the electricity and hydrogen energy can be managed across multiple interconnected subsystems to promote energy utilization performance. Thus, to improve the system energy supply reliability and utilization efficiency, the exploitation of an energy management solution for the MEMG considering the renewable generation uncertainties and the participation in the electricity market is demanded.

To this end, a hydrogen-based MEMG is exploited in this paper including multiple energy forms (i.e. electricity, hydrogen and heat) and multiple energy conversion and utilization devices, i.e. water electrolyzer (EL), fuel cell-based combined heat and power (FC-CHP), electricity boiler (EB) and heat storage system (HSS). A multiple time-scale coordinated energy management solution for the hydrogen-based MEMG participating in the electricity market is proposed to minimize the daily operational cost considering the electricity and hydrogen trading among subsystems. A collection of controllable facilities in the studied MEMG, e.g. EL, FC-CHP, EB and HSS, and electricity and hydrogen trading among subsystems enable the coordinated energy management of day-ahead scheduling and real-time dispatch. A MEMG composed of several subsystems, e.g., EHI-CSs and commercial parks, is considered as the case study to validate the proposed multiple time-scale and multiple energy-type coordinated energy management solution. The main technical contributions made in this work can be summarized threefold as follows:

(1) This work presented a multiple time-scale coordinated energy management solution to minimize the MEMG daily operational cost for a hydrogen-based MEMG in the presence of electricity, hydrogen and heating demands.
(2) Electricity and hydrogen energy transactions among subsystems in the MEMG are fully considered to implement flexible energy management and participation in the electricity market.
(3) The proposed solution is assessed through a case study of MEMG consisting of three EHI-CSs and a commercial park against a benchmark solution (i.e., no intra-day corrections), and the numerical results confirm its economic benefits.

The remainder of this paper is organized as follows: Section 2 describes related literature. Section 3 describes the hydrogen-based MEMG framework and the component modeling of hydrogen production and storage, FC-CHP, EB and HSS units. Section 4 presents the proposed multiple time-scale coordinated energy management solution. In Section 5 the proposed multiple time-scale energy management solution is assessed through test cases. Finally, the conclusion is made in Section 6.

2. Related work

In recent years, due to the high energy storage density and long lifetime of hydrogen-based storage technologies, the exploitation of hydrogen-based energy systems has attracted increasing attention with the breakthrough of hydrogen production, storage and transportation technologies [4]. A stochastic day-ahead scheduling model was proposed in [5] for microgrid energy management, while hydrogen storage systems in each microgrid were deployed for alleviating the renewable generation intermittences and dynamically balancing the energy throughout the day. In [6], to reduce wind generation power spillage and daily operation costs, the interaction between the price-based demand response and hydrogen storage systems was considered in the day-ahead market. In [7], for the hybrid energy system containing electricity, heating, cooling and hydrogen demands, a long-term optimal planning model and a model of seasonal hydrogen storage were proposed. As mentioned above, Hydrogen storage systems can convert low-cost or new energy generation into hydrogen through power-to-hydrogen (P2H) technology and generates electricity through hydrogen-to-power (H2P) technology when needed. On the other hand, the hydrogen produced can also be directly supplied to hydrogen demand, e.g. HFVs. The authors in [8] designed an off-grid charging station for supplying PEVs and HFVs, equipped with a PV system, diesel generator and hydrogen storage systems. The capacities of PV and diesel systems were optimal programming to minimize investment and operation costs. In [9], considering the distance and hydrogen selling price of the existing stations, a two-step pricing-based location approach for the new hydrogen fueling stations was proposed to maximize the profit of the new stations. The work in [10] proposed a cooperative operating model for wind turbines and hydrogen fueling stations that considers individual benefits, and the energy trading problem is solved using the Nash bargaining theory. An optimal scheduling model proposed in [11] for privately owned hydrogen fueling stations attempted to exploit the lower electricity market prices to decrease the power purchase cost and integrate the dynamic hydrogen pricing mechanisms to ensure the economic viability of the investment. In [12], considering an operating reserve market, a supervisory-based model for the optimal scheduling of distributed hydrogen fueling stations was proposed for supply to HFVs.

Further, the coupling utilization of multiple energy sources based on FC-CHP (i.e., hydrogen to electricity and heat) can effectively improve energy efficiency and energy supply reliability [13]. Hydrogen can be converted to electricity using a fuel cell with an efficiency of 40–60 %, while the FC-CHP systems, e.g., Polymer Electrolyte Membrane Fuel Cells (PEM-FC), can convert energy with an efficiency of up to 90 % [14]. Several studies have focused on the penetration of FC-CHP to co-supply local electricity and heat demands. In [15], a multi-objective optimization solution was proposed to offer optimal design parameters for the FC-CHP by considering the effect of degradation to maximize the efficiency of the FC-CHP. In [16], the authors proposed an energy management strategy for a microgrid with hydrogen fueling stations, electric vehicle parking lots and FC-CHP units. In [17], the authors presented a multi-criteria assessment of fuel cell-based residential combined cooling, heating and electricity system, and use a parametric analysis to optimize system performances, i.e. energy efficiency, annual cost and pollutant emission. In [18], an optimal heat and electricity dispatch of the FC-CHP-based microgrid was investigated considering the demand response to minimize the daily cost and emission. In [19], an optimization problem for the planning of a hydrogen-based microgrid was constructed to minimize annual capital and operation costs, and hydrogen to electricity, heat and cooling energy technology is considered to reduce the operation cost compared to the conventional electricity-driven energy system. A resilience-oriented operation model was proposed in [20] for industrial parks equipped with electricity, heat and hydrogen storage and FC-CHP unit, which aims to improve the resilience of electricity and heat demands under contingency status.

For the stable and economic operations of microgrids, the energy management strategy is essential to manage and coordinate dispatchable devices and energy trading with the utility grid for maintaining dynamic energy supply–demand balances [21]. The energy management solution for a single independent MEMG has been widely studied. For example, in [22] and [23], an energy planning problem was proposed for a MEMG considering different forms of energy storage and demand response to supply the electricity, heating and cooling loads. In [24], a risk-based bidding approach for a MEMG was proposed to assess the effectiveness of demand-side management. However, a microgrid consisting of several subsystems, or a multi-microgrid system, is considered more complex due to the coupling and interactions among subsystems. The appropriate coordination of energy exchange among these subsystems needs to be integrated to achieve the global optimization of operational objectives [25]. In [26], an energy trading optimization approach was proposed for a MEMG cluster considering demand response to realize cooperation among MEMGs. In [27], considering electricity trading among MEMGs, the hierarchical optimal configuration framework of a MEMG system was established to minimize the economic cost. It can be observed that the energy management of the multi-microgrid system in existing studies has considered the electrical transactions between microgrids. However, existing studies exploited the participation of microgrid integrated hydrogen in the electricity market without the consideration of the coordination among multiple subsystems. In this regard, for a hydrogen-based MEMG containing several interconnected subsystems, an energy management solution is proposed in this paper with consideration of both electricity and hydrogen linkage of subsystems.

Further, for the coordination and optimization operation of multiple forms of energy sources, e.g. electricity, hydrogen and heat, some corresponding energy management strategies are proposed in existing studies. However, the MEMG is a complex system with multiple forms of energy sources and multiple time-scale operational characteristics, which have not been fully considered in the existing studies, e.g., the same time scale is adopted for the energy dispatch among electricity, hydrogen and heat ([28,29]). In fact, the operation of hydrogen and heat energy generally varies at the hourly timescale, and the electricity energy dispatch needs to be carried out at a time scale of minutes [30]. In this regard, a multiple time-scale energy management solution is developed in this paper for managing and coordinating the electricity, hydrogen and heat energy in the MEMG. Besides, although, gaseous hydrogen pipelines are currently more suitable for long-distance transport, reference [31] indicated that as the hydrogen energy market matures, pipelines are gaining a cost advantage in hydrogen energy transportation. Thus, short-distance hydrogen pipeline transport would be a desirable option. Therefore, in this work, both electricity and hydrogen trading among the interconnected subsystems are considered to enhance the flexibility of hydrogen-based MEMG energy management.

3. Proposed model

3.1. Overview of the proposed system

In this work, the proposed hydrogen-based MEMG is shown in Fig. 1 (a), that composed of several interconnected subsystems and connected to the utility grid through a point of common coupling (PCC). As shown in the figure, four subsystems, i.e. three EHI-CSs and one commercial park energy system, are considered in this paper to implement the

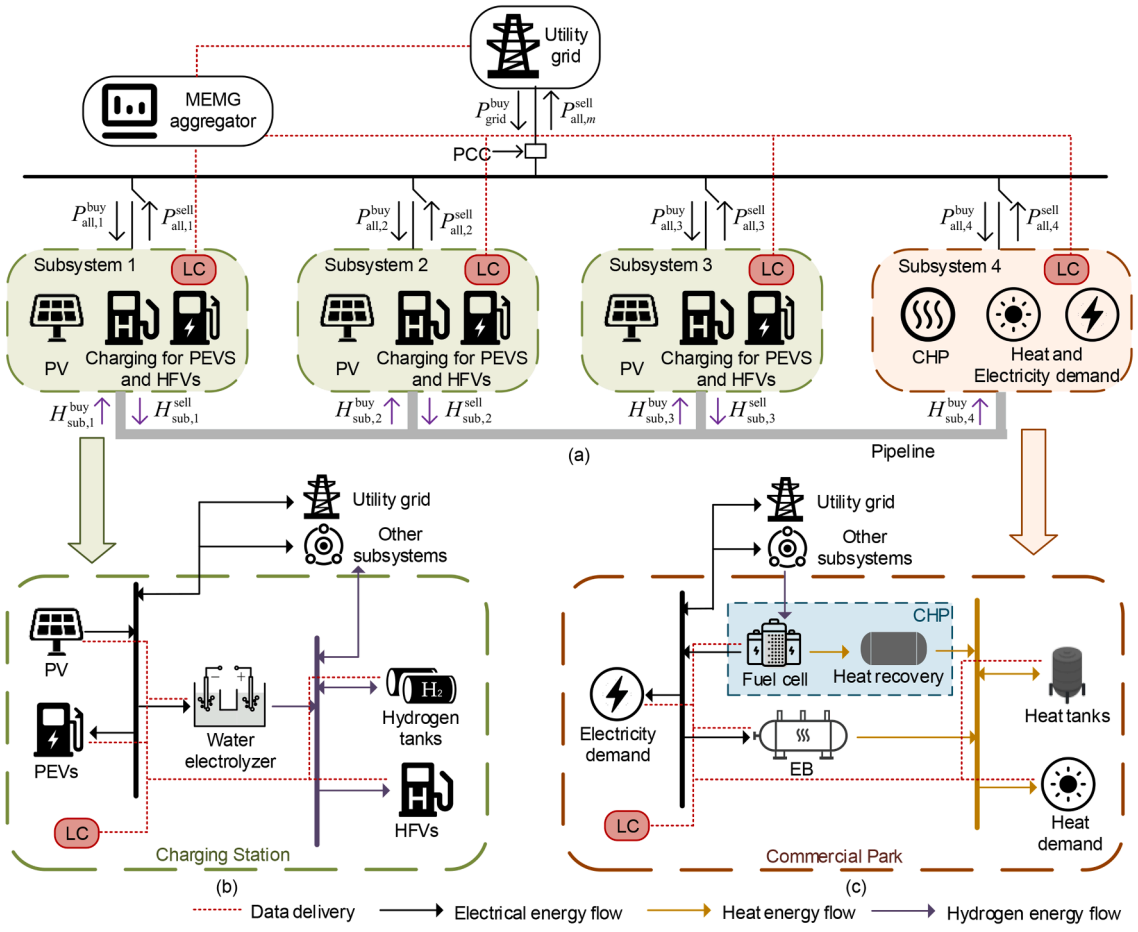

Fig. 1. Schematic illustration of MEMG: (a) MEMG with four subsystems; (b) EHI-CS for PEVs and HFVs; and (c) commercial park energy system.

energy management solution. It should be noted that the proposed solution can be used in the MEME consisting of a different number of subsystems with heterogeneous resources. In addition to absorbing or supplying electricity to the utility network, electricity and hydrogen energy can be transmitted between interconnected subsystems. Note that, the park energy system is not equipped with hydrogen production facilities and can only purchase hydrogen from EHI-CSs.

The structure of the EHI-CS is illustrated in Fig. 1(b) which consists of a PV power system, water electrolyzer, hydrogen storage tanks, and PEVs and HFVs demands. Such EHI-CSs can utilize renewable and inexpensive electricity to generate and store hydrogen and the stored hydrogen can later be used to serve the HFVs demand or sold to other subsystems to yield profit. The commercial park energy system considered in this work consists of an FC-CHP unit (including fuel cell and heat recovery system), EB, heat energy tanks, and electricity and heat demand, as illustrated in Fig. 1(c). The FC-CHP unit can meet both electrical and thermal demands using hydrogen and atmospheric oxygen. In addition to FC-CHP, heat demands can also be met by EB units, and residual heat can be stored in heat storage tanks.

The individual local controller (LC) in each subsystem is responsible for collecting the predicted and real-time data of local energy sources and loads within their associated subsystems and providing optimal management [32]. Meanwhile, to share electricity and hydrogen between subsystems to achieve supply–demand balance in the whole MEMG, available data in each LC of subsystems are delivered to the MEMG aggregator, which can make day-ahead scheduling and real-time operation considering objective function minimization.

3.2. EL unit

The EL unit is used to produce hydrogen by consuming electricity and water. The produced hydrogen by the EL unit needs to be pressurized to the required pressure before it can be stored in hydrogen tanks, which can be conventionally achieved with a mechanical compressor. However, pressurizing the hydrogen internally in the EL unit is an attractive option. For example, for a 200-bar PEM-EL, the output hydrogen pressure is 200 bar and can be directly stored in the hydrogen tank, eliminating the need for an external hydrogen compressor [33]. Moreover, reference [34] indicated that high-pressure EL has better efficiency compared to low-pressure EL with an external compressor. In this regard, the high-pressure EL device is considered in this paper and thus the model of the hydrogen compressor can be omitted. As far as this paper is concerned, the thermal model of the EL unit will be omitted for simplicity and temperature will be considered constant. This assumption also applies to the rest of the modeling in this work. The produced hydrogen by the EL is modeled by Eq.(1) and Eq. (2) denotes the upper and lower limits of hydrogen generated by the EL unit.

$$H_m^{EL}(t) = P_m^{P2H}(t) E^{P2H} \eta^{EL} \tag{1}$$

$$P_{\min}^{P2H} \leqslant P_m^{P2H}(t) \leqslant P_{\max}^{P2H} \tag{2}$$

where H_m^{EL} and P_m^{P2H} denote hydrogen production and power required by the EL unit; E^{P2H} is P2H conversion factor and η^{EL} is the efficiency of the EL unit; $P_{\max}^{\mathrm{P2H}}$ and $P_{\min}^{\mathrm{P2H}}$ represent the maximum and minimum input electric power of EL.

3.3. Hydrogen storage unit

The hourly stored hydrogen for the hydrogen storage tank is given by (3). It is calculated as the generation and purchased hydrogen minus the consumed and sold hydrogen in a subsystem. The generation of hydrogen is achieved from the EL unit and consumed hydrogen is used by HFVs. The storage of hydrogen is limited to the maximum and minimum tank capacity, as shown in Eq.(4), and hydrogen power charging/discharging of hydrogen storage tanks is limited as Eq. (5) [5].

$$HS_m(t) = HS_m(t-1) + H_m^{\mathrm{EL}}(t) - H_m^{\mathrm{HFV}}(t) + H_{\mathrm{sub},m}^{\mathrm{buy}}(t) - H_{\mathrm{sub},m}^{\mathrm{sell}}(t) \tag{3}$$

$$HS_{\min} \leqslant HS_m(t) \leqslant HS_{\max} \tag{4}$$

$$-H_{\max}^{\mathrm{HESS}} \leqslant HS_m(t) - HS_m(t-1) \leqslant H_{\max}^{\mathrm{HESS}} \tag{5}$$

where HS_m denotes stored hydrogen in the hydrogen tank; H_m^{HFV} is the hydrogen demand of HFVs; $H_{\mathrm{sub},m}^{\mathrm{buy}}$ $H_{\mathrm{sub},m}^{\mathrm{sell}}$ are hydrogen purchased and sold from the mth subsystem to other subsystems, respectively; $HS_{\max}$ and $HS_{\min}$ are the maximum and minimum value of hydrogen storage; $H_{\max}^{\mathrm{HESS}}$ is the maximum charging and discharging hydrogen limit of hydrogen tanks.

3.4. FC-CHP unit

With hydrogen and ambient oxygen, FC-CHP units can supply both electricity and heat demands, and the operational constraint of FC-CHP adopted in this work is shown in Eqs. (6)-(8), as suggested in [20]. The electrical power generated by FC-CHP can be calculated by Eq.(6), which is the multiplication of the hydrogen consumption、H2P conversion and electric generation efficiency, and should be restricted by Eq.(7). The FC-CHP unit has an applicable operation area, which means that the heat and electricity generated of the FC-CHP device are mutually restricted. the relationship between them is called the heat-to-electric ratio (d), which is assumed to be constant in this work and described as Eq.(8). More detailed constraints of the CHP unit can be found in [22].

$$P^{CHP}(t) = H^{CHP}(t) E^{H2P} r^{H2P} \tag{6}$$

$$0 \leqslant P^{CHP}(t) \leqslant P_{\max}^{CHP} \tag{7}$$

$$G^{CHP}(t) = P^{CHP}(t)/d \tag{8}$$

where H^{CHP}, P^{CHP} and G^{CHP} are Hydrogen consumption, electricity and heat power generated by the FC-CHP unit, respectively; $P_{\max}^{\mathrm{CHP}}$ is the maximum power generation limit of FC-CHP; E^{H2P} is the H2P conversion factor.

3.5. EB unit

To meet part of the heat demand, the EB can generate heat by consuming electricity. The heat power produced of EB can be modeled by Eq.(9), and the maximum heat power generated limit can be described in Eq.(10).

$$G^{\mathrm{EB}}(t) = P^{\mathrm{EB}}(t) \eta^{\mathrm{EB}} \tag{9}$$

$$0 \leqslant G^{\mathrm{EB}}(t) \leqslant G_{\max}^{\mathrm{EB}} \tag{10}$$

where G^{EB} and P^{EB} denote heat power generated and electricity consumption by the EB unit; η^{EB} is the efficiency of EB and $G_{\max}^{\mathrm{EB}}$ is the maximum heat power generation limited by the EB unit.

3.6. Hss

HSS containing a set of heat storage tanks and the stored heat power for heat storage tanks is given by (11), which is limited to the maximum and minimum tank capacity, as shown in Eq.(12). Heat power charging/discharging of the HSS model is limited as Eq. (13) [18].

$$GS(t) = GS(t-1) + G^{\mathrm{ch}}(t) - G^{\mathrm{dis}}(t) \tag{11}$$

$$GS_{\min} \leqslant GS(t) \leqslant GS_{\max} \tag{12}$$

$$-G_{\max}^{\mathrm{HSS}} \leqslant GS(t) - GS(t-1) \leqslant G_{\max}^{\mathrm{HSS}} \tag{13}$$

where GS denotes stored heat power in the heat storage tank; G^{ch} and G^{dis} represent the charging and discharging heat power; $GS_{\max}$ and $GS_{\min}$ are The maximum and minimum value of heat storage; $G_{\max}^{\mathrm{HSS}}$ is the maximum charging and discharging heat power limit of the HSS unit.

4. MEMG multiple Time-Scale energy management solution

The MEMG aggregator manages the MEMG and participates in both the day-ahead market (DM) and the real-time market (RTM). In the DM, the MEMG aggregator can estimate the one-day MEMG consumption profiles and makes them available to the market organizer which will produce the day-ahead electricity market based on the power demand and supply profiles [35]. Besides, the RTM is based on a dual-pricing market where power exchange deviations with the day-ahead scheduling are penalized. The inevitable difference between forecast data and real-time data may result in a considerable additional penalty for the power imbalance. In trading with the grid, electricity power consumed below the scheduled energy is penalized at a price lower than the day-ahead electricity market, whereas excess electricity power consumed is fined at a price higher than the day-ahead electricity market [36].

Within the MEMG aggregator, considering fluctuations of loads and renewable generations, an energy management solution is suggested to minimize the operation costs and create a supply–demand balance in the whole MEMG. As illustrated in Fig. 2(a), a multiple time-scale energy management solution is developed to achieve MEMG economic schedule by co-optimizing multiple energy-type and coordinating day-ahead scheduling and actual operation, as well as accommodating the fluctuation of renewable energy and loads. More specifically, the energy management solution is comprised of two stages, i.e. the day-ahead scheduling stage and the real-time dispatching stage. In the first stage, according to the day-ahead predicted data and the day-ahead electricity market, the MEMG aggregator conducts the day-ahead scheduling to determine its electricity purchase and sale with the utility grid. While during the actual operation stage, based on the intraday electricity market, a model predictive control (MPC) based operation model is proposed to mitigate the negative impact of the day-ahead predicting error.

Further, the hydrogen and heat demand generally varied at the hourly timescale, while the electricity demand fluctuates at a timescale of minutes. Thus, the energy management optimization problem can be transformed into slow timescale (STS) optimization and fast timescale (FTS) optimization. The index of STS and FTS are denoted by t_{s} andt_{f}, respectively. The timescale of hydrogen and heat energy real-time scheduling is 1 h (i.e. STS) and the rolling horizon of the dispatching spans to 4 h (in total 4 time slots); the timescale of real-time electrical dispatching is 15 min (i.e. FTS) and the rolling horizon of dispatching is 3 h (in total 12 time slots) [30]. The dispatching result of the first time slot is executed, and after completing a real-time dispatching decision, the rolling horizon moves forward by a one-time slot, as shown in Fig. 2 (b).

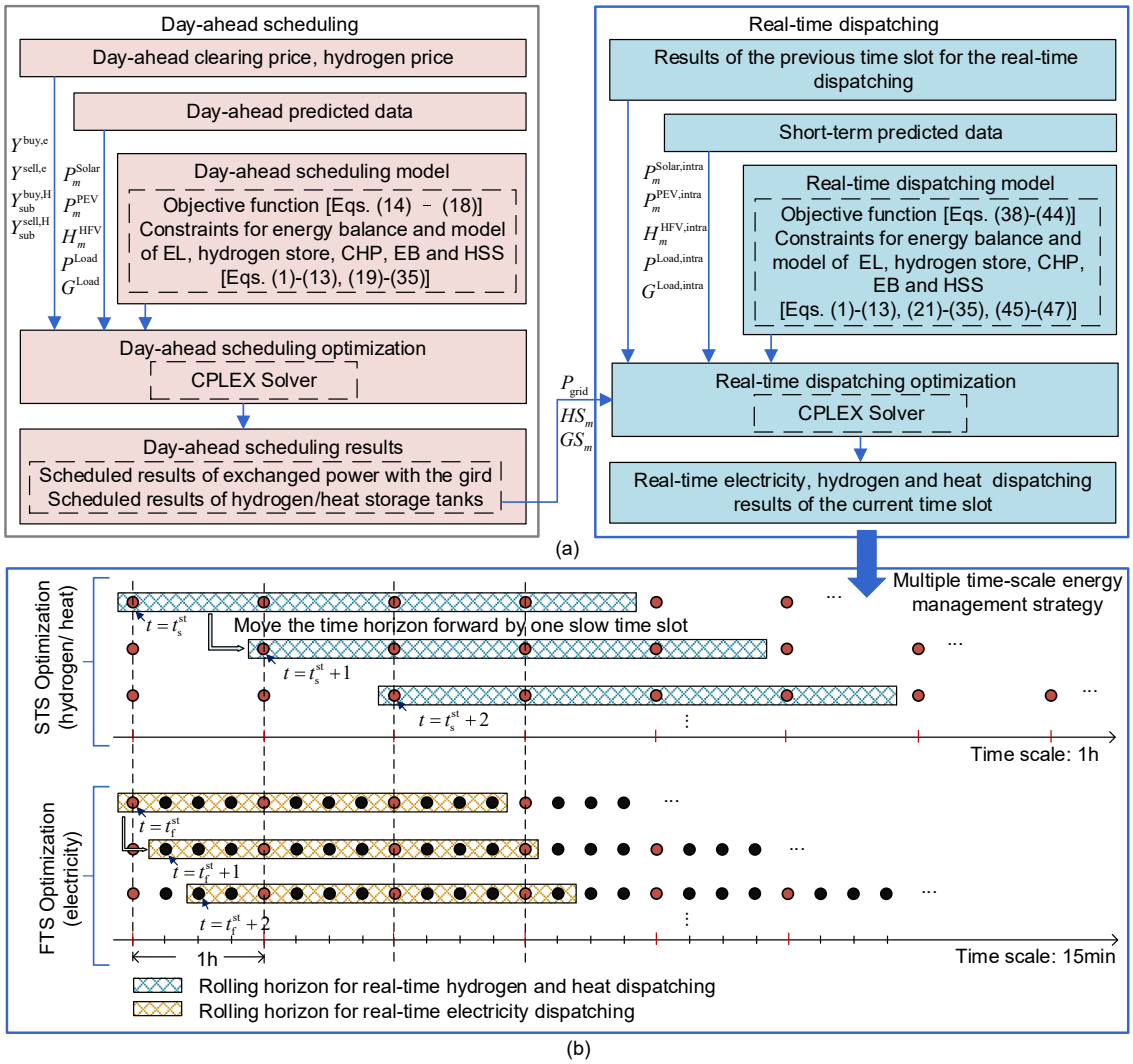

Fig. 2. Framework of the multiple time-scale energy management solution.

4.1. Day-ahead scheduling model

According to the day-ahead clearing price and the forecasted data of PV power generation, PEV and HFV charging demand and park energy load, the MEMG aggregator makes its economic optimization schedule to minimize the excepted value of the total daily operation cost, and the objective function is modeled by Eqs. (14)-(18). The objective function is represented in Eq. (14) which minimizes the total cost due to electricity and hydrogen trading and the component operating cost. Eq. (15) and Eq.(16) denote the cost of electric power trading (including the electrical transaction with the utility grid and between subsystems) and hydrogen power transaction cost, respectively. Eqs. (17) and (18) are the operating cost of the P2H and FC-CHP units, respectively.

$$\min OF = \sum_{t_s=1}^{T_s} \left(F^{e}(t_s) + F^{H}(t_s) + F^{P2H}(t_s) + F^{CHP}(t_s) \right) \Delta t_s \tag{14}$$

$$F^{e}(t_s) = \sum_{m=1}^{M} Y^{buy,e}(t_s) P^{buy}_{all,m}(t_s) - Y^{sell,e}(t_s) P^{sell}_{all,m}(t_s) \tag{15}$$

$$F^{H}(t_s) = \sum_{m=1}^{M} Y^{buy,H}_{sub}(t_s) H^{buy}_{sub,m}(t_s) - Y^{sell,H}_{sub}(t_s) H^{sell}_{sub,m}(t_s) \tag{16}$$

$$F^{P2H}(t_s) = \sum_{m=1}^{M} \left(b^{P2H} P^{P2H}_{m}(t_s) + c^{P2H} \right) I^{P2H}_{m}(t_s) \tag{17}$$

$$F^{CHP}(t_s) = b^{CHP} P^{CHP}(t_s) \tag{18}$$

where $Y^{buy,e}$ and $Y^{sell,e}$ are the price of buying and selling electricity of day-ahead clearing price; $Y^{buy,H}_{sub}$ and $Y^{sell,H}_{sub}$ are the price of buying and selling hydrogen; $P^{sell}_{all,m}$ and $P^{buy}_{all,m}$ are the total electrical power purchased and sold for the mth subsystem, respectively; I^{P2H}_{m} is the binary status indicator of P2H process in the EL unit and $I^{P2H}_{m} = 1$ indicates that EL unit is working, otherwise idling; b^{P2H} and c^{P2H} are the cost function coefficient of the P2H mode and the b^{CHP} is the cost function coefficients of the FC-CHP unit.

The supply–demand balance of electricity, hydrogen and heat energy, the constraints of electricity and hydrogen transportation, and the operational constraints of each component in the MEMG are considered as follows:

(1) Electricity supply–demand balance:

The electricity supply–demand balance for mth subsystems including each EHI-CS and the park system in each time slot is defined as Eqs.(19) and (20), respectively. The electricity balance constraint requires that

the electric power generated by source generations minus the electricity demands equal the electricity sold or purchased by the subsystem.

$$P^{\text{Solar}}_{\text{used},m}(t_s) - P^{\text{P2H}}_{m}(t_s) - P^{\text{PEV}}_{m}(t_s) = P^{\text{sell}}_{\text{all},m}(t_s) - P^{\text{buy}}_{\text{all},m}(t_s) \tag{19}$$

$$P^{\text{CHP}}(t_s) - P^{\text{EB}}(t_s) - P^{\text{Load}}(t_s) = P^{\text{sell}}_{\text{all},m}(t_s) - P^{\text{buy}}_{\text{all},m}(t_s) \tag{20}$$

where $P^{\text{Solar}}_{\text{used},m}$ denotes PVs power generation utilized in actual and P^{Load} denotes the electrical demand of the park energy system.

(2) Electricity transportation constraints:

The electrical power balance constraints of the whole MEMG can be described in Eq. (21).

$$P^{\text{buy}}_{\text{grid}}(t_s) - P^{\text{sell}}_{\text{grid}}(t_s) = \sum_{m=1}^{M}(P^{\text{buy}}_{\text{all},m}(t_s) - P^{\text{buy}}_{\text{sub},m}(t_s)) - \sum_{m=1}^{M}(P^{\text{sell}}_{\text{all},m}(t_s) - P^{\text{sell}}_{\text{sub},m}(t_s)) \tag{21}$$

where $P^{\text{buy}}_{\text{grid}}$ and $P^{\text{sell}}_{\text{grid}}$ are electrical power purchased and sold from the utility grid; $P^{\text{buy}}_{\text{sub},m}$ and $P^{\text{sell}}_{\text{sub},m}$ are electrical power purchased and sold from the mth subsystem to other subsystems. As described in Eq. (22), two binary status indicators $I^{\text{buy}}_{\text{grid}}$ and $I^{\text{sell}}_{\text{grid}}$ are introduced to guarantee the MEMG cannot receive and send power to the utility grid simultaneously. Eqs. (23) and (24) are used to ensure that the transmission of electricity between the MEMG and the utility grid cannot exceed the line limitation (f_L) in the PCC.

$$I^{\text{buy}}_{\text{grid}}(t_s) + I^{\text{sell}}_{\text{grid}}(t_s) \leqslant 1 \tag{22}$$

$$0 \leqslant P^{\text{buy}}_{\text{grid}}(t_s) \leqslant f_L \times I^{\text{buy}}_{\text{grid}}(t_s) \tag{23}$$

$$0 \leqslant P^{\text{sell}}_{\text{grid}}(t_s) \leqslant f_L \times I^{\text{sell}}_{\text{grid}}(t_s) \tag{24}$$

(3) Heat supply–demand balance:

The heat power balance constraint of the park energy system requires that the heat generated by EB (G^{EB}) and FC-CHP (G^{CHP}) minus the heating demands (G^{Load}) equals the heat absorbed and released by the HSS, which can be expressed as Eq.(25).

$$G^{\text{EB}}(t_s) + G^{\text{CHP}}(t_s) + G^{\text{dis}}(t_s) = G^{\text{Load}}(t_s) + G^{\text{ch}}(t_s) \tag{25}$$

(4) Hydrogen transportation constraints:

Hydrogen can be piped among subsystems. For the pipeline option, according to [37] and [38], it is assumed that the pipeline diameter is 0.3 m, the average pressure in the pipeline is 2 MPa, and the maximum gas flow rate in the pipeline is 30 m/s. Thus, the hydrogen transport volume limit is about$7.6 \times 10^3\ \text{m}^3/\text{h}$. Based on the ideal gas law, the relationship between gas volume and mass is shown in Eq.(26).

$$pV = nRT \tag{26}$$

where, p is the gas pressure; V is the gas volume; T is the temperature; R is the gas constant, which is equal to$8.31\ J/(mol{\cdot}k)$; and n is the number of moles of the gas, which can be found by the equation$n = m/M$, where m is the mass is the gas and M is the molar mass. In this paper, the operation temperature is considered as a constant, set as 298 K [39], to simplify the evaluation of the proposed energy management solution. Based on Eq. (26), the mass-based hydrogen transport constraint can be obtained, i.e.,$H^{trans}_{\max} = 121.88\ kg/h$.

Two binary variables $I^{\text{H,buy}}_{m}$ and $I^{\text{H,sell}}_{m}$ are introduced in Eq. (27) to ensure that one subsystem does not purchase and sell hydrogen to other subsystems, simultaneously. Hydrogen power purchased/sold by each subsystem is limited in Eq. (28) and Eq. (29), and the hydrogen power transfer among subsystems is limited in Eq. (30). The balance model of hydrogen power purchase and sale between subsystems is shown in Eq. (31).

$$I^{\text{H,buy}}_{m}(t_s) + I^{\text{H,sell}}_{m}(t_s) \leqslant 1 \tag{27}$$

$$0 \leqslant H^{\text{buy}}_{\text{sub},m}(t_s) \leqslant H^{\text{trans}}_{\max} \times I^{\text{H,buy}}_{m}(t_s) \tag{28}$$

$$0 \leqslant H^{\text{sell}}_{\text{sub},m}(t_s) \leqslant H^{\text{trans}}_{\max} \times I^{\text{H,sell}}_{m}(t_s) \tag{29}$$

$$0 \leqslant H^{\text{trans}}_{\text{sub},m_1m_2}(t_s) \leqslant H^{\text{trans}}_{\max} \tag{30}$$

$$\sum_{m=1}^{M} H^{\text{buy}}_{\text{sub},m}(t_s) = \sum_{m=1}^{M} H^{\text{sell}}_{\text{sub},m}(t_s) \tag{31}$$

where $H^{\text{trans}}_{\text{sub},m_1m_2}$ denotes the hydrogen transfer from m_1th subsystem to m_2th subsystem.

(5) Component operation constraints:

The operation constraints of EL, hydrogen storage, FC-CHP, EB and HSS units are shown in Eqs. (1) to (13). Moreover, in the first time slot of the day, the amount of hydrogen/heat in hydrogen/heat storage tanks is given in Eqs.(32) and (34), and to have the same flexibility scheduling on every scheduling day, Eqs. (33) and (35) specify that the initial value of the stored hydrogen/heat at $t_s = 0$ is the same as the value at$t_s = T_s$.

$$HS_m(0) = HS_{m,\text{ini}} \tag{32}$$

$$HS_m(T_s) = HS_m(0) \tag{33}$$

$$GS(0) = GS_{\text{ini}} \tag{34}$$

$$GS(T_s) = GS(0) \tag{35}$$

where $HS_{m,\text{ini}}$ and GS_{ini} are the initial hydrogen and heat storage values, respectively. The expected value of the electricity power exchanged between MEMG and the utility grid (P_{grid}) is expressed as Eq. (36), which should be obeyed during the real-time operation; otherwise, the utility grid can enforce a penalty on MEMG.

$$P_{\text{grid}}(t_s) = P^{\text{buy}}_{\text{grid}}(t_s) - P^{\text{sell}}_{\text{grid}}(t_s) \tag{36}$$

4.2. Real-time dispatch model

The hydrogen and heat demand usually fluctuates at the hourly timescale (i.e. STS) and the electrical energy varies at the timescale of minute (i.e. FTS) [30]. The relationship between STS and FTS can be described as Eq. (37), which can be interpreted as the FTS time slot $t_f(t_f \in [z(t_s - 1) + 1, zt_s])$ belonging to the STS time slot t_s[40].

$$z = \Delta t_s / \Delta t_f \tag{37}$$

where Δt_s and Δt_f are the time interval of STS and FTS, respectively.

In the real-time dispatching stage, the MEMG aggregator should decrease the penalty cost to achieve its profit maximization in the RTM participation through controllable facilities and adjustment methods in the MEMG. Notice, in the real-time dispatching, the electricity and hydrogen trading between each subsystem and the operation of EL and FC-CHP may different from day-ahead scheduling. Hence, the objective function of the MEMG for RTM participation should contain the penalty cost of energy imbalance, as well as the transaction cost between each subsystem and the component operation cost. For the STS and FTS optimization problems, the objective functions are shown in Eq. (38) and (39), respectively. After obtaining the SFS optimization results of

the time slott_s, only the electricity dispatching order of the first FTS time slot, i.e.$t_f = z(t_s - 1) + 1$, in the STS time slot t_s is actually implemented.

$$\min OF_{\mathrm{STS}}^{\mathrm{RTM}} = \sum_{t_s=t_s^{\mathrm{st}}}^{T_s} \begin{pmatrix} F^{\mathrm{e,RTM}}(z(t_s-1)+1) + F^{\mathrm{H,RTM}}(t_s) \\ +F^{\mathrm{P2H,RTM}}(t_s) + F^{\mathrm{CHP,IBM}}(t_s) \end{pmatrix} \Delta t_s \tag{38}$$

$$\min OF_{\mathrm{FTS}}^{\mathrm{RTM}} = \sum_{t_f=t_f^{\mathrm{st}}}^{T_f} \begin{pmatrix} F^{\mathrm{e,RTM}}(t_f) + F^{\mathrm{H,RTM}}([t_f/z]) \\ +F^{\mathrm{P2H,RTM}}([t_f/z]) + F^{\mathrm{CHP,RTM}}([t_f/z]) \end{pmatrix} \Delta t_f \tag{39}$$

where, the extra superscript "RTM" denotes the cost of the RTM participation. The function "$[\cdot]$" is used to round up to the smallest integer not less than the variable. Different from the day-ahead scheduling model, as shown in Eq. (40), the electricity power transaction cost in the RTM participation includes the penalty cost of energy imbalance and the electrical transaction cost between subsystems. The expected energy imbalance to be compensated in the RTM is modeled as Eqs.(41) to (43) [36]. Eq. (44) represents the cost for each subsystem due to the electrical trading between subsystems. Notice, in the real-time dispatching stage, the exchange of electricity between the subsystems in the MEMG will continue at a previously agreed price (i.e. day-ahead clearing price). Further, the extra superscript "in" represents the values used in the intraday dispatch model that was already established in the day-ahead scheduling model.

$$F^{\mathrm{e,RTM}}(t_f) = C_{\mathrm{grid}}^{\mathrm{im}}(t_f) + \sum_{m=1}^{M} C_{\mathrm{sub},m}^{\mathrm{e,RTM}}(t_f) \tag{40}$$

$$C_{\mathrm{grid}}^{\mathrm{im}}(t_f) = \begin{cases} Y^{\mathrm{im,below}}([t_f/z]) \times P^{\mathrm{im}}(t_f), & P^{\mathrm{im}}(t_f) \leqslant 0 \\ Y^{\mathrm{im,excess}}([t_f/z]) \times P^{\mathrm{im}}(t_f), & P^{\mathrm{im}}(t_f) \geqslant 0 \end{cases} \tag{41}$$

$$P_{\mathrm{grid}}^{\mathrm{im}}(t_f) = P_{\mathrm{grid}}^{\mathrm{in}}(t_f) - P_{\mathrm{grid}}([t_f/z]) \tag{42}$$

$$P_{\mathrm{grid}}^{\mathrm{in}}(t_f) = P_{\mathrm{grid}}^{\mathrm{buy,in}}(t_f) - P_{\mathrm{grid}}^{\mathrm{sell,in}}(t_f) \tag{43}$$

$$C_{\mathrm{sub},m}^{\mathrm{e,RTM}}(t_f) = Y^{\mathrm{buy,e}}([t_f/z]) P_{\mathrm{sub},m}^{\mathrm{buy,in}}(t_f) - Y^{\mathrm{sell,e}}([t_f/z]) P_{\mathrm{sub},m}^{\mathrm{sell,in}}(t_f) \tag{44}$$

where $P_{\mathrm{grid}}^{\mathrm{im}}$ is the imbalance power of the deviation between the day-ahead schedule and real-time dispatch. The expressions of$F_t^{\mathrm{H,RTM}}$, $F_t^{\mathrm{P2H,RTM}}$ and $F_t^{\mathrm{CHP,RTM}}$ are similar to Eqs. (16)-(18). Due to the penalty cost of energy imbalance, light abandonment may occur in the PV system, which is subjected to (45). Due to the different time-scale of electricity and hydrogen/heat, the electricity balance constraints in the real-time dispatching model should be enforced by Eqs. (46) and (47).

$$0 \leqslant P_{\mathrm{used},m}^{\mathrm{Solar}} \leqslant P_m^{\mathrm{Solar}} \tag{45}$$

$$P_{\mathrm{used},m}^{\mathrm{Solar}}(t_f) - P_m^{\mathrm{P2H,in}}([t_f/z]) - P_m^{\mathrm{PEV,in}}(t_f) = P_{\mathrm{all},m}^{\mathrm{sell,in}}(t_f) - P_{\mathrm{all},m}^{\mathrm{buy,in}}(t_f) \tag{46}$$

$$P^{\mathrm{CHP,in}}([t_f/z]) - P^{\mathrm{EB,in}}([t_f/z]) - P^{\mathrm{Load,in}}(t_f) = P_{\mathrm{all},m}^{\mathrm{sell,in}}(t_f) - P_{\mathrm{all},m}^{\mathrm{buy,in}}(t_f) \tag{47}$$

Also, the operational constraints of each component are given in Eqs. (1)-(13) need to be met, as well as constraints Eqs. (21)-(35) described in the day-ahead scheduling model. For the sake of limited space, these equations are not repeated here.

5. Simulations and numerical results

In this work, to evaluate and validate the efficiency of the suggested multiple time-scale energy management solution, a hydrogen-based MEMG test system with four subsystems (i.e. three EHI-CSs and one commercial park) has been constructed. In the test system, three EHI-CSs consist of three PV systems with the rated power of 2.4 MW, 5.2 MW and 2.8 MW, and three charging facilities for PEVs with the maximum charging capacities of 1.0 MW, 0.6 MW and 0.6 MW, three fueling facilities for HEVs with maximum fueling capacities of 70 kg, 30 kg, and 30 kg, respectively. The commercial park in the test system consists of electricity and heat demands with a rated capacity of 1.8 MW and 1.5 MW, respectively. The parameters of the EL, hydrogen storage, FC-CHP, HES and EB unit are given in Table 1, as suggested in [41], [42] and [6], and the capacity of the PCC (f_L) is 6 MW. The following parameter values are chosen in the day-ahead scheduling stage to leave some space for MEMG real-time dispatching: $P_{\max}^{\mathrm{P2H}} = 2.4$ MW, $HS_{\max}/HS_{\min} = 240/36$ kg, $H_{\max}^{\mathrm{HESS}} = 120$ kg, $P_{\max}^{\mathrm{CHP}} = 0.8$ MW, $G_{\max}^{\mathrm{EB}} = 0.32$ MW, $GS_{\max}/GS_{\min} = 2.4/0.12$ MW, $G_{\max}^{\mathrm{HSS}} = 0.8$ WM and$f_L = 4.8$ MW [43]. The day-ahead clearing price used in this test study is shown in Fig. 3(a), which is obtained from ISO New England history data [44]. It is considered that the day-ahead selling price is 0.9 times the day-ahead purchasing price, i.e. $Y^{\mathrm{sell,e}} = 0.9Y^{\mathrm{buy,e}}$ [45], and the positive/negative imbalance price is 2/0.8 times the day-ahead purchasing price, i.e. $Y^{\mathrm{im,excess}}(t_f) = 2Y^{\mathrm{buy,e}}([t_f/z])$ and$Y^{\mathrm{im,below}}(t_f) = 0.8Y^{\mathrm{buy,e}}([t_f/z])$, respectively [46]. Also, the selling price of hydrogen is considered to be 0.95 times of purchasing price, i.e.$Y_{\mathrm{sub}}^{\mathrm{sell,H}} = 0.95Y_{\mathrm{sub}}^{\mathrm{buy,H}}$, and$Y_{\mathrm{sub}}^{\mathrm{sell,H}} = 2.4$ \$/kg [47].

The real data for PV systems generation, PEV demands, HFV demands, park electricity and heat demands used in the test day are displayed in Fig. (b) to (f), which are extracted from [10] and [48] to [51]. The predicted data is obtained by adding a forecast error to the real data. The power forecasting errors of PVs are considered to follow beta distributions, and the stochastic variables of load power variations are assumed to follow normal distributions[52]. Further, due to the similar environment, it is assumed that the power forecast errors in each subsystem follow the same distribution [29], and the predictions are with the normalized root mean squared error of 10 %, as suggested in [50] and [53]. Further, the intra-day prediction is carried out on a short-term scale (4 h), assuming that the short-term predicted data is close to the actual value [54]. Thus, in this work, real data is used for the first four hours of the rolling horizon, and day-ahead predicted data is used for the remaining time slots.

All the programs are performed in MATLAB (version 2018a) and executed on a computer equipped with a 3.20 GHz i7-97000 CPU and 16.00 G RAM. The executive time for decision-making of the day-ahead scheduling is 5.01 s, and the average executive for real-time dispatching for one one-time slot decision-making is 2.05 s.

5.1. Day-ahead MEMG scheduling results

Based on the day-ahead clearing price and the prediction data, day-ahead scheduling is performed. The MEMG net-load profile, as well as the electricity exchanged with the utility grid of each subsystem, are shown in Fig. 4, and the MEMG net-load profile will be utilized as the baseline for the actual operation. Note that the positive value represents the electricity purchased by the utility grid, while the negative value represents electricity sold to the utility grid. It shows that the purchased electricity is increased obviously, owing to the P2H process, which could enhance the power utilization of the utility grid during low-price periods if there is no PV power generation.

Further, the day-ahead scheduling for the supply–demand balance of

Table 1
The required parameters for modeling the system.

Parameter	Value	Parameter	Value
$P_{\max}^{\mathrm{P2H}}/P_{\min}^{\mathrm{P2H}}$ (MW)	3/ 0.3	E^{H2P}(kWh/ kg)	39.4
$HS_{\max}/HS_{\min}$ (kg)	300/ 30	η^{EL}	0.8
$H_{\max}^{\mathrm{HESS}}$(kg)	150	r^{H2P}	0.36
$P_{\max}^{\mathrm{CHP}}$(MW)	1	d	0.7
$G_{\max}^{\mathrm{EB}}$(MW)	0.4	η^{EB}	0.95
$GS_{\max}/GS_{\min}$(MW)	3/0.3	b^{P2H}(\$/kWh)	0.0141
$G_{\max}^{\mathrm{HSS}}$(MW)	1.0	c^{P2H}(\$/h)	15.99
E^{P2H}(kg /kWh)	0.0254	b^{CHP}(\$/kWh)	0.02

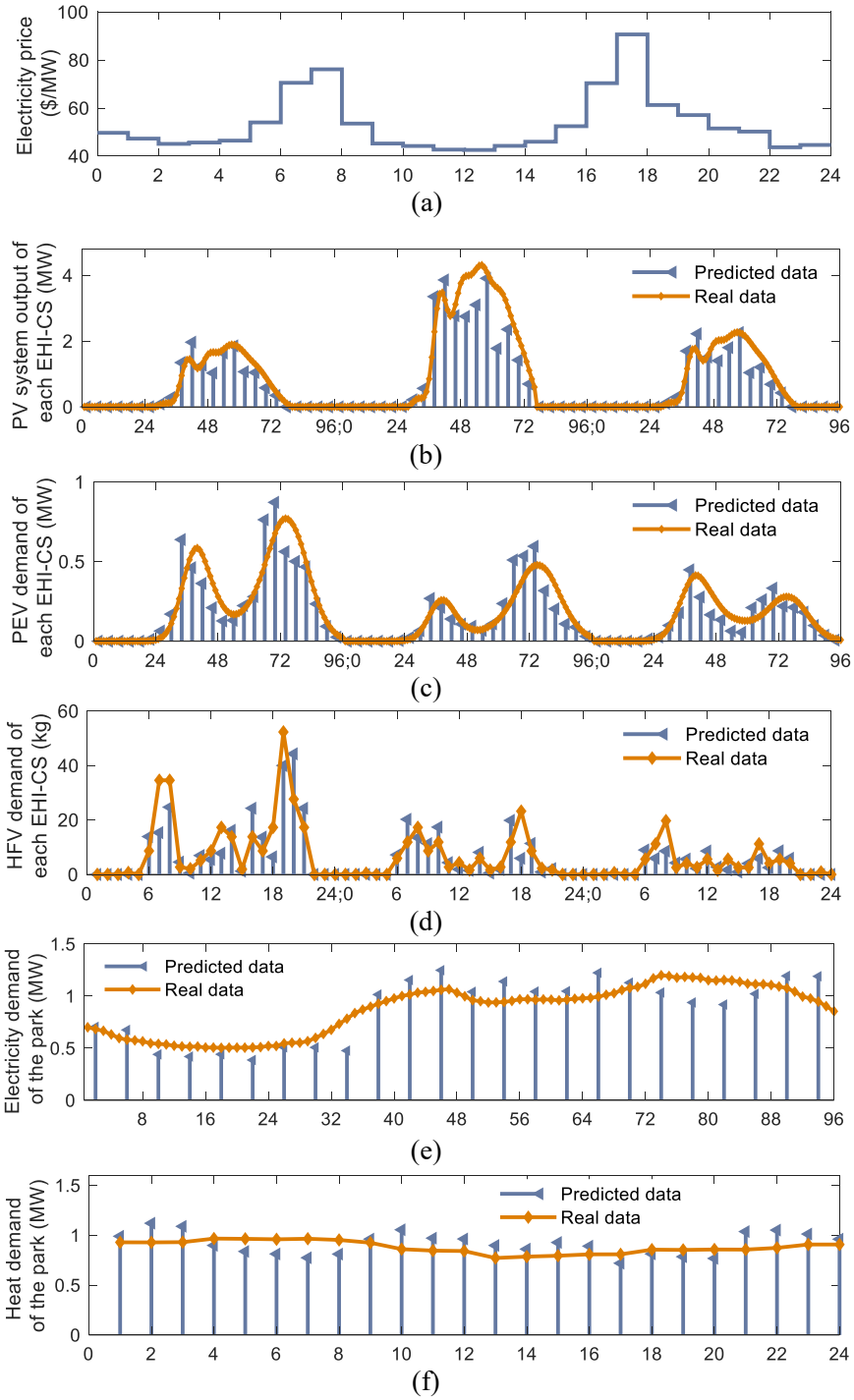

Fig. 3. (a) Day-ahead electricity price; predicted and real data for (b) PV systems output; (c) PEV demands; (d) HFV demands; (e) park electricity demand; and (f) park heat demand.

electricity, hydrogen and heat energy of each subsystem in the MEMG are presented in Fig. 5, Fig. 6 and Fig. 7 respectively. From Fig. 5, for each EHI-CS, the PV power generation and electricity purchased are the main electricity power sources. Apart from supplying for PEVs demand, electricity can produce hydrogen and be sold to the utility grid or other subsystems. The commercial park energy system, since it generates little electricity, mostly buys electricity from outside and rarely sells electricity. From Fig. 6, the hydrogen demands are mainly met through hydrogen production by P2H technology and hydrogen discharging from hydrogen storage tanks for EHI-CSs, and the excess hydrogen can be stored or sold to other subsystems. The hydrogen purchased in the commercial park is to meet the FC-CHP unit to generate electricity and heat energy. For heat balance in the commercial park, as shown in Fig. 7, both FC-CHP and EB can produce heat energy to supply the park's heat demands. Since the ratio of heat and electricity generation in FC-CHP is fixed, surplus heat can be generated during the production of electricity and stored by the HSS.

5.2. *Real-time MEMG dispatching results*

After day-ahead scheduling, multiple time-scale MPC is used in the real-time dispatching stage to update the MEMG's control actual

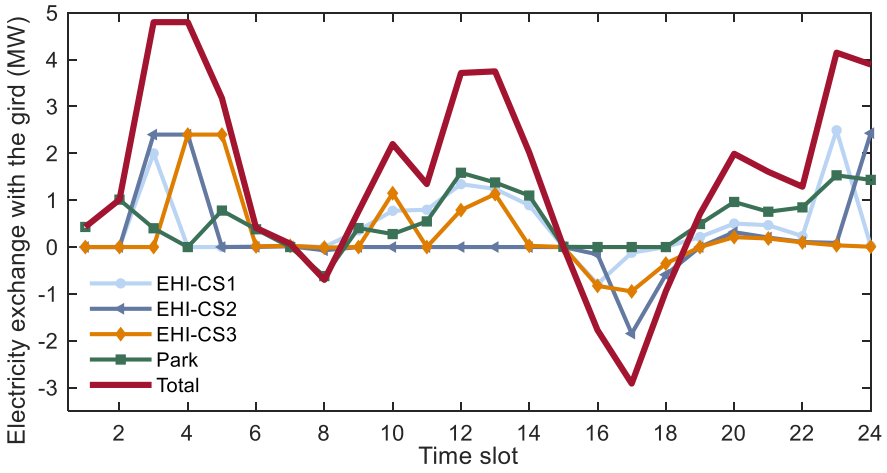

Fig. 4. Day-ahead scheduled MEMG net-load.

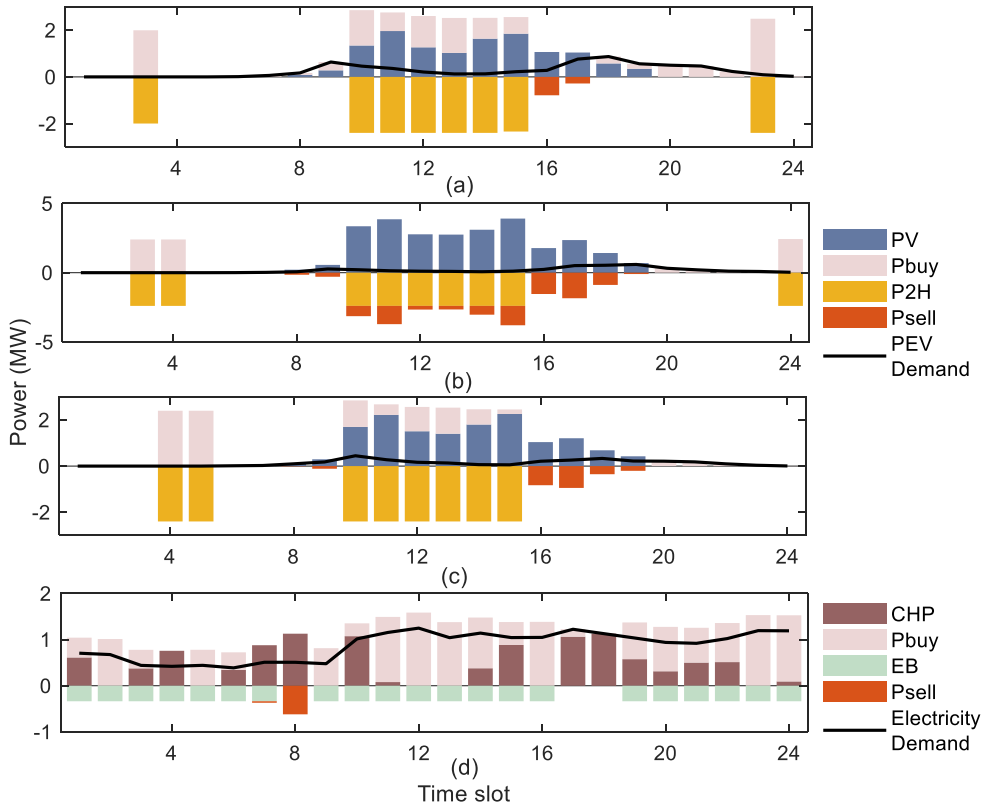

Fig. 5. MEMG electricity balance by the day-ahead scheduled of (a) EHI-CS1; (b) EHI-CS2; (c) EHI-CS3; and (d) commercial park.

operation based on short-term predicted data, and the actual MEGE net-load profiles are given in Fig. 8. Also, the actual operating results of electricity, hydrogen and heat of each subsystem in the MEMG, are presented in Fig. 9, Fig. 10 and Fig. 11, respectively. The results demonstrate the effectiveness of real-time dispatching in accommodating renewable energy supply fluctuations as well as the uncertainty of electricity, hydrogen and heat demands. Further, the numerical results of real-time dispatching show that, due to the inevitable error of day-ahead and short-term prediction, some deviations exist between the day-ahead scheduling and the real-time optimization results.

Further, to verify the economic performance of the suggested multiple time-scale energy management solution for the MEMG, a benchmark solution is adopted as the comparison: the MEMG's day-ahead scheduling is strictly executed in the real-time operation stage without MPC update. Fig. 12 presents the actual daily operation cost over 7 test days for the MEMG with two different solutions. In detail, the average actual daily operation cost of the proposed MPC-based energy management solution for the MEMG is 2265.1 $, which is 37.08 % lower than the benchmark (3105.1 $). It's also worth noting that the penalty cost in the real-time operation of the proposed solution is smaller than the benchmark solution. This indicates that in addition to controllable facilities (i.e. EL, FC-CHP and EB units), the multiple EHI-CSs units include an adjustment method in the proposed solution, i.e. electricity and hydrogen transportation between subsystems, allowing flexible

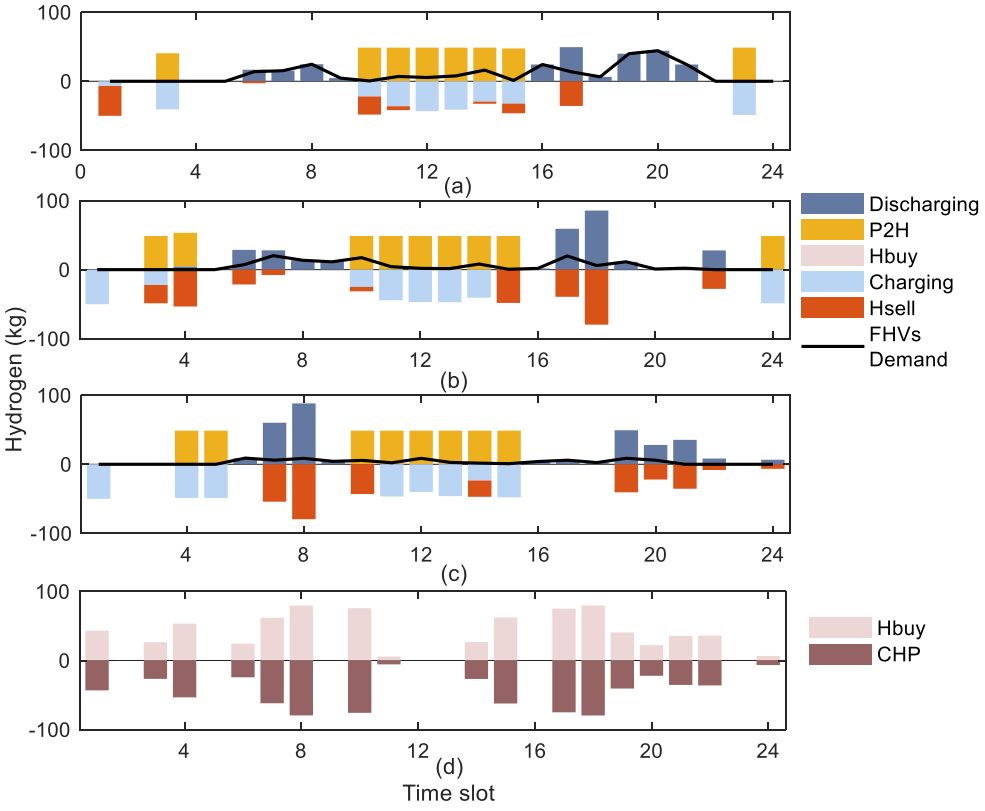

Fig. 6. MEMG hydrogen balance by the day-ahead scheduled of (a) EHI-CS1; (b) EHI-CS2; (c) EHI-CS3; and (d) commercial park.

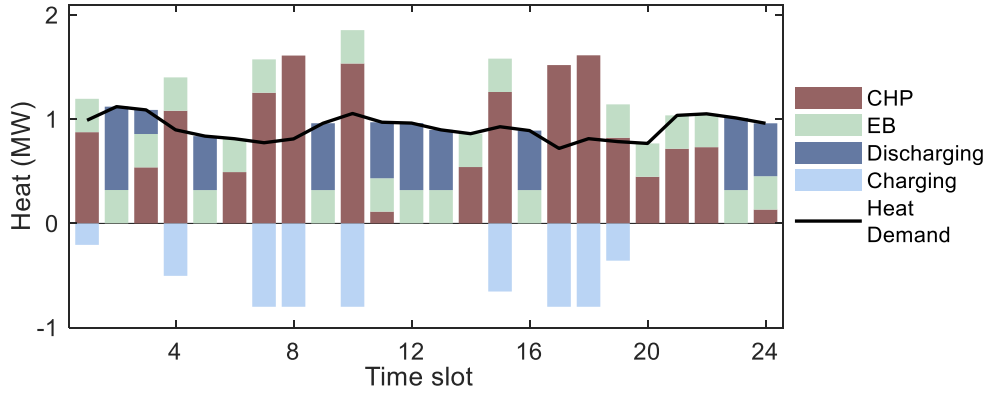

Fig. 7. Heat balance of the commercial park by the day-ahead scheduled.

coordination of day-ahead scheduling and real-time dispatching. In comparison to the benchmark solution, Fig. 13 shows the MEMG net-load results of the suggested MPC-based energy management solution. It is found that the net-load profile obtained by the MPC-based energy management solution is much closer to the day-ahead scheduling compared with the benchmark. This indicates that the proposed MPC-based multiple time-scale energy management solution can effectively mitigate the effects of renewable energy and demand uncertainties. However, some significant deviation between day-ahead net-load and MPC-based energy management solution results still occurs in certain time slots, such as time slots 17–20, 281–284 and 409–412. This is due to the inevitable difference between day-ahead prediction and the actual power generation and demands, i.e., prediction errors. Although the rolling horizon in MPC can address the challenge with the prediction errors, some impacts caused by large prediction errors cannot be eliminated.

6. Conclusions and future work

In this paper, a multiple time-scale energy management solution is proposed for a hydrogen-based MEMG with several interconnected subsystems (EHI-CSs and commercial park). With consideration of renewable energy and demand uncertainties, the energy management solution aims to minimize the expected operation cost of the MEMG in the real-time electricity market. In the MEMG, multiple energy-type and a collection of controllable facilities (e.g., EL, FC-CHP, EB and HSS units) enable energy management to coordinate day-ahead scheduling and real-time dispatch. Meanwhile, electricity and hydrogen energy trading between interconnected subsystems can also enhance the flexibility of MEMG energy management. Further, the proposed energy management

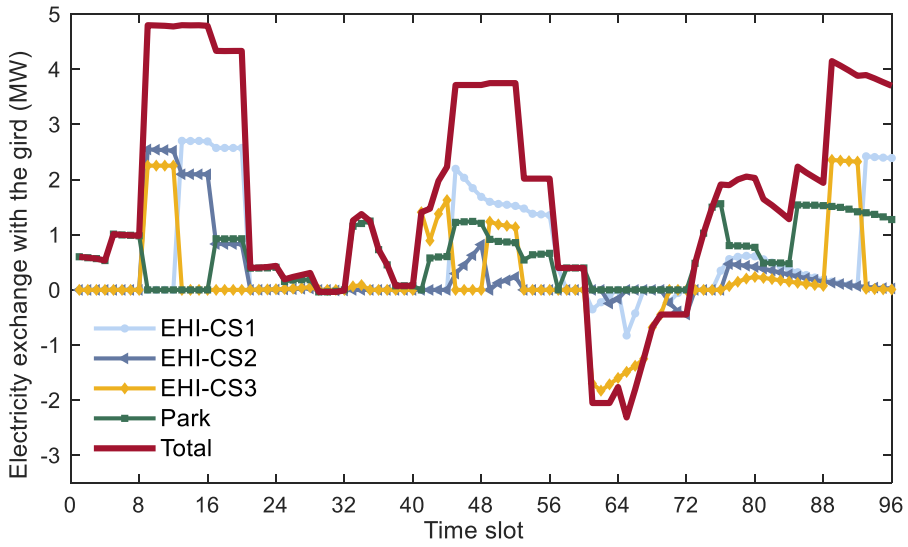

Fig. 8. Actual MEMG net-load profiles.

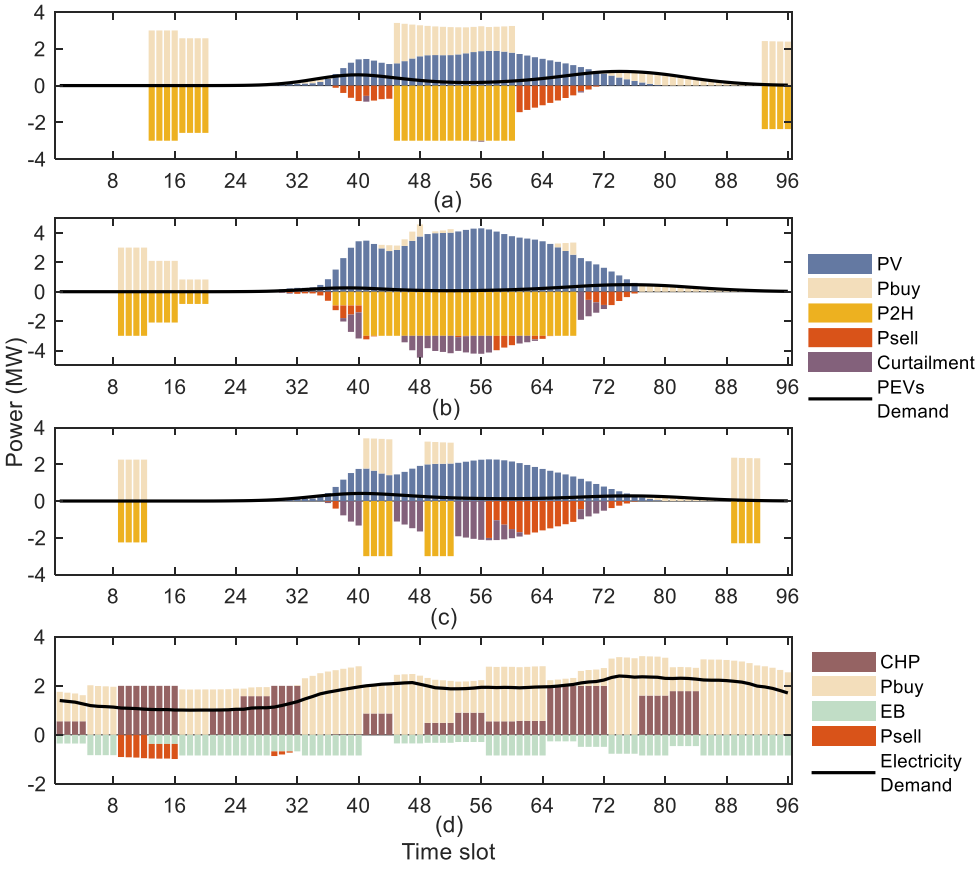

Fig. 9. MEMG electricity balance by the actual operation of (a) EHI-CS1; (b) EHI-CS2; (c) EHI-CS3; and (d) commercial park.

solution has been validated through a hydrogen-based MEMG test system with four subsystems. It should be noted that the proposed energy management solution can have a wide range of applications and can be used universally in similar problems with inter-connected energy networks. Numerical results show that the proposed multiple time-scale coordinated energy management solution outperforms the benchmark solution with additional economic benefit, i.e. reduction of the actual operational costs by an average of 37.08 %.

For future work, the following research directions are considered worth further research effort.

(1) The electricity market has been fully considered in this work with different electricity pricing, but the hydrogen market is not explicitly considered and the hydrogen price is set as a constant price. In this regard, the dynamic pricing schemes of hydrogen

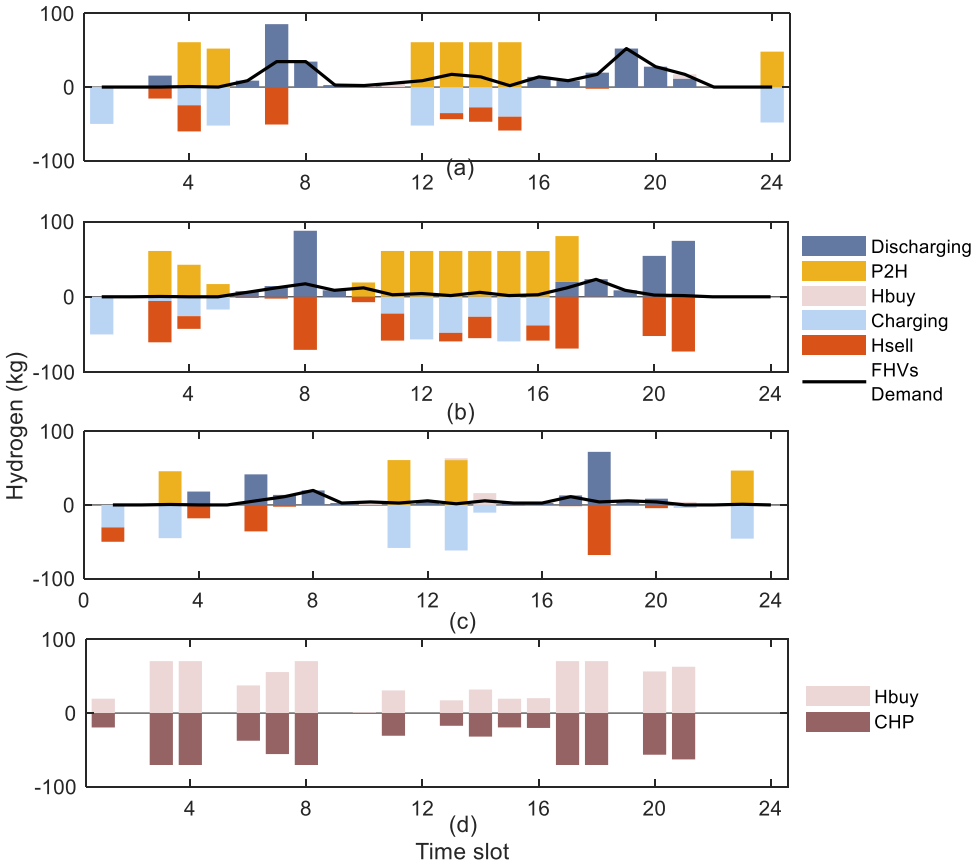

Fig. 10. MEMG hydrogen balance by the actual operation of (a) EHI-CS1; (b) EHI-CS2; (c) EHI-CS3; and (d) commercial park.

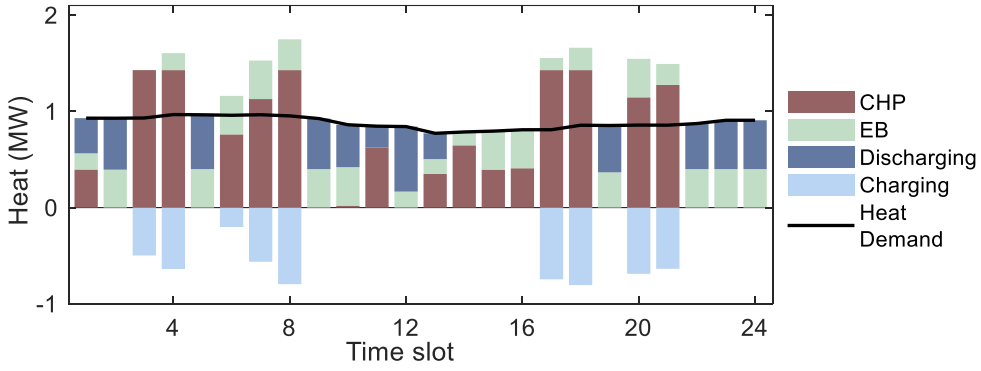

Fig. 11. Heat balance of the commercial park by the actual operation.

during transactions can be further considered in the energy management strategy for a hydrogen-based MEMG.

(2) The hydrogen can be produced in large production plants or directly generated on-site locally. Due to the limitation of current hydrogen demand and the huge initial infrastructure investment of long-distance pipelines, the on-site production option is considered attractive as it can avoid transportation and infrastructure investment and improve the utilization of distributed renewable generation. However, with the development of hydrogen-based technologies and the dramatic increase in social hydrogen demand, the cost of hydrogen transportation is likely to change drastically in the future, and MEMGs can choose to purchase low-price hydrogen from the hydrogen market. Thus, coordination of on-site hydrogen production and purchasing hydrogen from the hydrogen market needs to be further studied to achieve better utilization of local distributed generation and minimize the overall operating cost of the MEMG.

(3) The electricity purchased from the utility grid can be procured from non-renewable sources, which can result in carbon emissions. To improve the utilization of renewable generation to produce hydrogen and reduce the carbon emissions of the system, capacity planning of renewable generation and storage systems in a MEMG needs to be further studied.

CRediT authorship contribution statement

Xiaolun Fang: Conceptualization, Methodology, Data curation. **Wei Dong:** Investigation. **Yubin Wang:** Visualization. **Qiang Yang:**

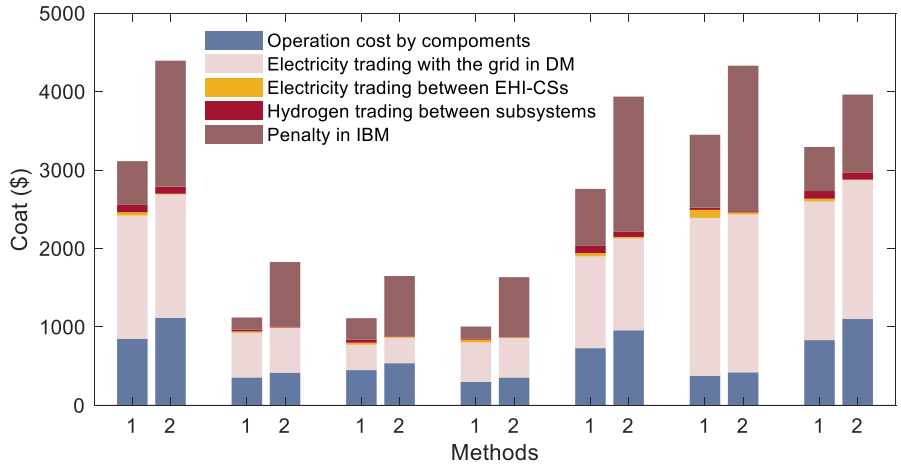

Fig. 12. Comparison of the operational cost over 7 test days. Note, 1: suggested solution; 2: benchmark solution.

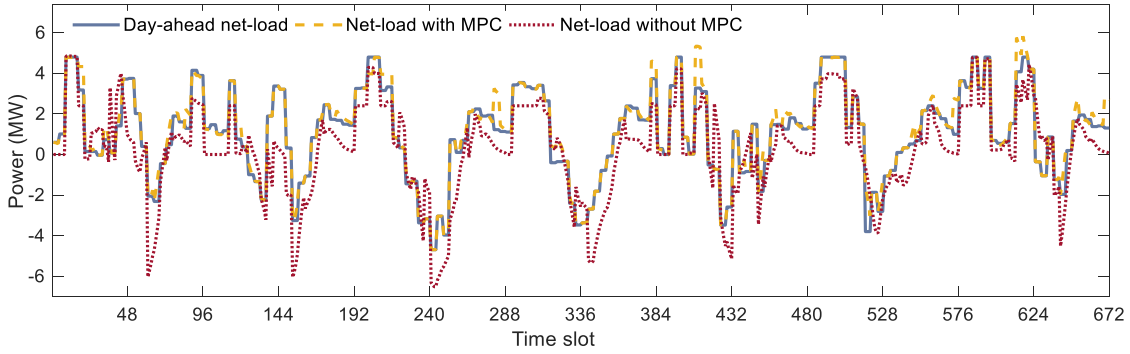

Fig. 13. The MEMG net-load results of day-ahead scheduling and real-time dispatching with and without MPC.

Supervision.

Declaration of Competing Interest

The authors declare that they have no known competing financial interests or personal relationships that could have appeared to influence the work reported in this paper.

Data availability

No data was used for the research described in the article.

Acknowledgements

This work is supported by the Natural Science Foundation of China (52177119) and the Technology Research and Development Program of Zhejiang Province (2022C01239).

References

[1] Banaei M, Rafiei M, Boudjadar J, Khooban M. A Comparative Analysis of Optimal Operation Scenarios in Hybrid Emission-Free Ferry Ships. IEEE Trans Transp Electrif March 2020;6(1):318–33.
[2] Wang X, Li B, Wang Y, Lu H, Zhao H, Xue W. A bargaining game-based profit allocation method for the wind-hydrogen-storage combined system. Appl Energy 2022;310.
[3] Tabandeh A, Hossain MJ, Li L. Integrated multi-stage and multi-zone distribution network expansion planning with renewable energy sources and hydrogen refuelling stations for fuel cell vehicles. Appl Energy 2022;319.
[4] Bolun Xu, et al. Modeling of lithium-ion battery degradation for cell life assessment. IEEE Trans Smart Grid 2016;9:1131–40.
[5] Daneshvar M, Ivatloo BM, Zare K, Asadi S. Transactive energy management for optimal scheduling of interconnected microgrids with hydrogen energy storage. Int J Hydrogen Energy 2021;46(30):16267–78.
[6] Mirzaei MA, Yazdankhah AS, Ivatloo BM. Stochastic security-constrained operation of wind and hydrogen energy storage systems integrated with price-based demand response. Int J Hydrogen Energy 2019;44(27):14217–27.
[7] Pan G, Gu W, Lu Y, Qiu H, Lu S, Yao S. Optimal Planning for Electricity-Hydrogen Integrated Energy System Considering Power to Hydrogen and Heat and Seasonal Storage. IEEE Trans Sustainable Energy 2020;11(4):2662–76.
[8] Mehrjerdi H. Off-grid solar powered charging station for electric and hydrogen vehicles including fuel cell and hydrogen storage. Int J Hydrogen Energy 2019;44 (23):11574–83.
[9] Thiel D. A pricing-based location model for deploying a hydrogen fueling station network. Int J Hydrogen Energy 2020;45(46):24174–89.
[10] Wu X, Li H, Wang X, Zhao W. Cooperative Operation for Wind Turbines and Hydrogen Fueling Stations With On-Site Hydrogen Production. IEEE Trans Sustainable Energy 2020;11(4):2775–89.
[11] El-Taweel NA, Khani H, Farag HEZ. Hydrogen Storage Optimal Scheduling for Fuel Supply and Capacity-Based Demand Response Program Under Dynamic Hydrogen Pricing. IEEE Trans Smart Grid 2019;10(4):4531–42.
[12] Khani H, El-Taweel NA, Farag HEZ. Supervisory Scheduling of Storage-Based Hydrogen Fueling Stations for Transportation Sector and Distributed Operating Reserve in Electricity Markets. IEEE Trans Ind Inf 2020;16(3):1529–38.
[13] Yan N, et al. Energy Management Method of Electricity Heat Hydrogen Multi-Coupling System for Retired Power Battery Echelon Utilization in Microgrids. IEEE Trans Appl Supercond Nov. 2021;31(8):1–5.
[14] Herrmann A, Madlow A, Krause H. Key performance indicators evaluation of a domestic hydrogen fuel cell CHP. Int J Hydrogen Energy 2019;44:19061–6.
[15] Yang Y, Zhang H, Yan P, Jermsittiparser K. Multi-objective optimization for efficient modeling and improvement of the high temperature PEM fuel cell based Micro-CHP system. Int J Hydrogen Energy 2020;45:6970–81.
[16] Saatloo AM, Ebadi R, Mirzaei MA, et al. Multi-objective IGDT-based scheduling of low-carbon multi-energy microgrids integrated with hydrogen refueling stations and electric vehicle parking lots. Sustain Cities Soc 2021;74.
[17] Chena X, Zhou H, Li W, et al. "Multi-criteria assessment and optimization study on 5 kW PEMFC based residential CCHP system. Energy Convers Manage 2018;160: 384–95.

[18] Didani HP, Nojavan S, Nourollahi R, Zare K. Optimal economic-emission performance of fuel cell/CHP/storage based microgrid. Int J Hydrogen Energy 2019;44:6896–908.
[19] Liu J, Xu Z, Wu J, Liu K, Guan X. Optimal planning of distributed hydrogen-based multi-energy systems. Appl Energy 2021;281.
[20] Liu J, Cao X, Xu Z, Guan X, Dong X, Wang C. Resilient operation of multi-energy industrial park based on integrated hydrogen-electricity-heat microgrids. Int J Hydrogen Energy 2021;46:28855–69.
[21] Zhou B, et al. Multi-microgrid Energy Management Systems: Architecture, Communication, and Scheduling Strategies. J Mod Power Syst Clean Energy May 2021;9(3):463–76.
[22] Nosratabadi SM, Hemmati R, Jahandide M. Eco-environmental planning of various energy storages within multi-energy microgrid by stochastic price-based programming inclusive of demand response paradigm. J Energy Storage 2021; 36.
[23] Nosratabadi SM, Hemmati R, Gharaei PK. Optimal planning of multi-energy microgrid with different energy storages and demand responsive loads utilizing a technical-economic-environmental programming. Int J Energy Res 2020;45: 6985–7017.
[24] Nosratabadi SM, Moshizi HN, Guerrero JM. Strategy for demand side management effectiveness assessment via a stochastic risk-based bidding approach in a multi-energy microgrid containing combined cooling, heat and power and photovoltaic units. IET Renew Power Generation 2022; 16: pp.2036-2058.
[25] Li P, Wang Z, Wang J, Guo T, Yin Y. A multi-time-space scale optimal operation strategy for a distributed integrated energy system. Appl Energy 2021;289.
[26] Wu Q, Xie Z, Ren H, Li Q, Yang Y. Optimal trading strategies for multi-energy microgrid cluster considering demand response under different trading modes: A comparison study. Energy 2022;254.
[27] Zhao J, Wang W, Guo C. Hierarchical optimal configuration of multi-energy microgrids system considering energy management in electricity market environment. Int J Electr Power Energy Syst 2023;144.
[28] Lakouraj MM, Niaz H, Liu JJ, Siano P, Moghaddam AA. Optimal risk-constrained stochastic scheduling of microgrids with hydrogen vehicles in real-time and day-ahead markets. J Cleaner Prod 2021;318.
[29] Wu X, Qi S, Wang Z, Duan C, Wang X, Li F. Optimal scheduling for microgrids with hydrogen fueling stations considering uncertainty using data-driven approach. Appl Energy 2019; 253.
[30] Bao Z, Zhou Q, Yang Z, Yang Q, Xu L, Wu T. A Multi Time-Scale and Multi Energy-Type Coordinated Microgrid Scheduling Solution—Part I: Model and Methodology. IEEE Trans Power Syst 2015;30(5):2257–66.
[31] Liu H, Ma J. A review of models and methods for hydrogen supply chain system planning. *CSEE J Power Energy Syst* early access 2020:1–12.
[32] Nikmehr N, Ravadanegh SN, Khodaei A. Probabilistic optimal scheduling of networked microgrids considering time-based demand response programs under uncertainty. Appl Energy 2017;198:267–79.
[33] Hancke R, Holm T, Ulleberg Ø. "The case for high-pressure PEM water electrolysis. "*Energy Conversion and Management* 2022;261.
[34] Salehmin MNI, Husaini T, Goh J, Sulong AB. High-pressure PEM water electrolyser: A review on challenges and mitigation strategies towards green and low-cost hydrogen production. Energy Convers Manage 2022;268.
[35] Zheng Y, Yu H, Shao Z, Jian L. Day-ahead bidding strategy for electric vehicle aggregator enabling multiple agent modes in uncertain electricity markets. Appl Energy 2020;280.
[36] Das S, Basu M. Day-ahead optimal bidding strategy of microgrid with demand response program considering uncertainties and outages of renewable energy resources. Energy 2020;190:1–13.
[37] Gerboni R. "11 - Introduction to hydrogen transportation," *Compendium of Hydrogen*. Energy 2016:283–99.
[38] How to calculate pressure, velocity and flow in pipeline design, Avaliable at [Online]: https://www.comateflowmeter.com/calculate-pressure-velocity-flow-in-pipeline-design/.
[39] Takahashi K. Transportation of Hydrogen by pipeline. Energy Carriers and Conversion Systems, vol.2, 2016.
[40] Liu Y, Zhang Y, Chen K, Chen SZ, Tang B. Equivalence of Multi-Time Scale Optimization for Home Energy Management Considering User Discomfort Preference. IEEE Trans Smart Grid 2017;8(4):1876–87.
[41] Petrollese M, Valverde L, Cocco D, Cau G, Guerra J. Real-time integration of optimal generation scheduling with MPC for the energy management of a renewable hydrogen-based microgrid. Appl Energy 2016;166:96–106.
[42] Agency, U. S. Environmental Protection. "Catalog of CHP Technologies," 2014.
[43] Bao Z, Zhou Q, Yang Z, Yang Q, Xu L, Wu T. A Multi Time-Scale and Multi Energy-Type Coordinated Microgrid Scheduling Solution—Part II: Optimization Algorithm and Case Studies. IEEE Trans Power Syst 2015;30(5):2267–76.
[44] ISO New England. Day-Ahead Hourly Locational Marginal Price,accessed on Feb. 10, 2016. [Online]. Available: http://www.iso-ne.com/isoexpress/web/reports/pricing/-/tree/lmps-da-hourly.
[45] Yu L, Jiang T, Cao Y. Energy Cost Minimization for Distributed Internet Data Centers in Smart Microgrids Considering Power Outages. IEEE Trans Parallel Distrib Syst 2015;26(1):120–30.
[46] Wang Y, Dong W, Yang Q. "Multi-stage optimal energy management of multi-energy microgrid in deregulated electricity markets. Appl Energy 2022;310.
[47] Bertuccioli L, Chan A, Hart D, et al. Development of Water Electrolysis in the European Union. New Energy World, 2014.
[48] University of Queensland. Weather and Local Environment. [Online]. Available: http://www.uq.edu.au/solarenergy/pv-array/weathe.
[50] Dong W, Yang Q, Li W, Zomaya AY. Machine Learning based Real-time Economic dispatch in Islanding Microgrids in a Cloud-Edge Computing Environment. IEEE Internet Things J 2021;8(17):13703–11.
[51] Li R, Nahaei SS. Optimal operation of energy hubs integrated with electric vehicles, load management, combined heat and power unit and renewable energy sources. J Energy Storage 2022; 48.
[52] Dong W, Yang Q, Fang X, Ruan W. Adaptive optimal fuzzy logic based energy management in multi-energy microgrid considering operational uncertainties. Appl Soft Comput J 2021;98.
[53] Ge X, Shi L, Fu Y, et al. Data-driven spatial-temporal prediction of electric vehicle load profile considering charging behavior. Electr Power Syst Res 2020;187: 106469.
[54] Luo F, Ranzi G, Wan C, Xu Z, Dong ZY. A Multistage Home Energy Management System With Residential Photovoltaic Penetration. IEEE Trans Ind Inf 2019;15(1): 116–26.

Further reading

[49] Sun S, Yang Q, Yan W. Hierarchical optimal planning approach for plug-in electric vehicle fast charging stations based on temporal-SoC charging demand characterisation. IET Gener Transm Distrib 2018;12:4388–95.